MNRAS 000, 1–6 (2018) Preprint 3 October 2018 Compiled using MNRAS LATEX style file v3.0

Detecting the Cosmic Web: LyA Emission from Gas Filaments at z=3

Lydia M. Elias,[1★] Shy Genel,[2] Amiel Sternberg[2,3] Julien Devriendt[4] Adrianne Slyz[4]
[1]*Department of Physics and Astronomy, University of California Riverside, 900 University Ave., Riverside, 92521*
[2]*Center of Computational Astrophysics, 162 5th Ave., New York, NY, 10010*
[3]*Raymond and Beverly Sackler School of Physics and Astronomy, Tel Aviv University, Ramat Aviv 69978, Israel*
[4]*Department of Physics, University of Oxford, Keble Road, Oxford OX1 3RH, UK*

Accepted XXX. Received YYY; in original form ZZZ

ABSTRACT
Our standard cosmological model (LCDM) predicts the existence of the cosmic web: a distribution of matter into filaments connecting galaxies. However, observational evidence of the cosmic web has been elusive due to the extremely low surface brightness levels of the filaments. The recent deep MUSE/VLT data (Bacon et al. 2017) as well as upcoming observations offer a promising avenue for Lyα detection, but require theoretical context. We use hydrodynamical cosmological simulations at two different resolutions to investigate the detectability of the filaments feeding a Lyα-bright halo ($M_* = 10^{13}$) at z=3. We find that stacking is insufficient to detect the halo's filaments with MUSE. However, by degrading the resolution of the image from $(0.2")^2$ to $(5.3")^2$ a filament is easily detected. We also find that while recombination processes are responsible for the majority of the Lyα emission, most detectable emission is due to collisional excitation.

Key words: keyword1 – keyword2 – keyword3

1 INTRODUCTION

Cosmological simulations have long suggested the presence of diffuse filaments of both dark and baryonic matter between galaxies (Peebles and Groth 1975; Klypin and Shandarin 1983; Haider et al. 2016). However, it is only recently that the contribution of the cosmic web to galactic evolution has been fully appreciated. Specifically, at z≥2, the primary mode of matter accretion for a galaxy is now understood to be through filamentary streams of cold (10^4 K) gas that feed into the dark matter halo (Dekel et al. 2009).

Unfortunately, the low matter density of the streams prohibits star formation, making observation nearly impossible. The difficulty of detection is further exacerbated by the expansion of the universe, which 'stretches' the filaments, decreasing their density. Simulations consistently show that filaments are therefore at their densest and most detectable at z≃3 (Fardal et al. (2001)). Despite the difficulties, some tentative detections have been made. For example, Swinbank et al. (2015) report a detection of an extended (≃ 150kpc) Lyα halo at z=4.1 using MUSE. Zheng et al. (2018), and Battaia et al. (2018) report discoveries of enormous Lyα nebulae at z=2.45 and z=3 with end-to-end sizes of 232kpc and 297kpc, respectively.

However, even in a new era of deeper observations, a statistically robust sample of detections remains elusive. In Gallego et al. (2018), 390 oriented subcubes of the deepest MUSE/VLT data (~30 hrs of exposure, reaching surface brightness levels of 3.9×10^{-19}ergs^{-1}cm^{-2} Bacon et al. (2017)) are stacked without finding detectable Lyα emission in the IGM. Furthermore, Rosdahl and Blaizot (2010) investigate the detectability of extended Lya emission using cosmological zoom simulations and find that the Lyα luminosity is concentrated in the central 20% of the halo radius. This paper aims to investigate detectability of Lyα emission from cold gas streams using a large volume cosmological hydrodynamical simulation. In Section 2.1 we detail the simulation used, in Section 2.2 we describe the Lyα emission processes, in Section 3 we present the results of our investigation, and in Section 4 we state the conclusions of the project.

2 SIMULATIONS AND METHODS

2.1 Simulations

Two simulations were used for the analysis: one with low resolution and one with high resolution. The low resolution simulation has mass per particle of $1.0\times10^7 M_\odot$ and $1.6\times10^6 M_\odot$ for dark matter and baryons, respectively and a gravitational softening length of 1kpc. The high resolution simula-

★ E-mail: lydia.elias@email.ucr.edu (LME)

tion has mass per particle of $1.3\times10^6 M_\odot$ and $2.0\times10^5 M_\odot$ for dark matter and baryons, respectively and a gravitational softening length of 0.5kpc. Both boxes have side lengths of ≃35 Mpc and were run with the moving mesh code AREPO (Springel 2010). They are consistent with WMAP-9 standard cosmology, with Ω_m=0.2726, Ω_b=0.0456, Ω_Λ=0.7274, and H_0=70.4km/s/Mpc (Hinshaw et al. 2013).

Gas cell cooling and heating are consistent with Illustris 1 (Vogelsberger et al. 2014a). Above a density threshold of $n_H = 0.2\mathrm{cm}^{-3}$, gas follows an equation of state that is used to implicitly treat the multiphase structure of the ISM Springel and Hernquist (2003). Cold and dense gas above this threshold becomes eligible for star formation with a timescale proportional to the local density. No feedback or black holes are modeled in either simulation. Halos and galaxies are identified using the SUBFIND algorithm (Springel et al. 2001; Dolag et al. 2009). In short, groups are first identified based only on particle positions using the Friends of Friends (FoF) algorithm and gravitationally self-bound structures are later identified within groups by using SUBFIND. The object sitting at the center of the gravitational potential of each halo is called the central or host galaxy and all other substructures associated with the group will be referred to as satellites or subhalos.

2.2 Lyα Emission

Lyman α emission can originate from two processes: collisional excitation and recombination. We assume an optically-thin limit as we are interested in detections from diffuse filaments far from the main halo.

Collisional Excitation

When a free electron collides with a H atom, the electron within the atom is excited to a higher energy level before cascading back to the ground state. In the process a Lyα photon is emitted. Lyα emission from collisional excitation, j_{col}, in units of $\mathrm{cm}^{-3}\mathrm{s}^{-1}$ was modeled as:

$$j_{col} = q_{col}(T) * n_e * n_H \tag{1}$$

where q_{col} is the collisional ionization coefficient given in (Dijkstra (2017)) as $q_{col} = (8.63 * 10^{-6}) \times e^{-E/kT}/2\sqrt{T}\mathrm{cm}^3\mathrm{s}^{-1}$, n_e is the electron number density, and n_H is the neutral hydrogen number density.

Recombination

When a free electron combines with a free proton, it cascades from a high energy level to a lower, more stable energy level, possibly emitting a Lyα photon. Lyα emission from recombination, j_{rec}, in units of $\mathrm{cm}^{-3}\mathrm{s}^{-1}$ was modeled as:

$$j_{rec} = \alpha(T) * n_e * n_p \tag{2}$$

where α is the case A recombinational coefficient $\alpha = 1.68 \times T^{-0.85}\mathrm{cm}^3\mathrm{s}^{-1}$ where temperature dependence is given in Osterbrock and Ferland (2006) and is normalized to agree with Faucher-Giguere et al. (2010). n_p is proton density and remaining variables are defined above.

Temperature dependence of collisional and recombinational emission is shown in Fig. 1. At larger temperatures,

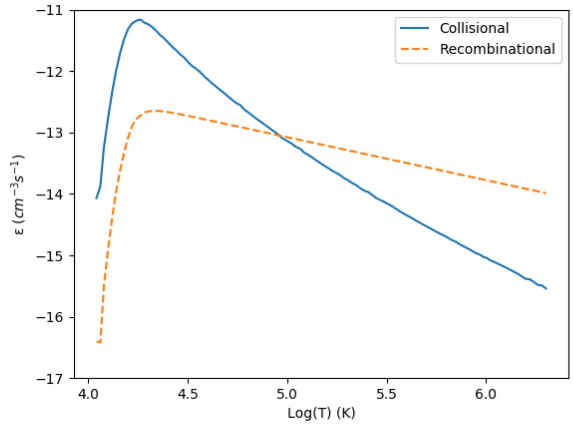

Figure 1. Temperature dependence of collisional and recombinational processes resulting in Lyα emission.

the gas becomes completely ionized and recombinational processes dominate, while at low temperatures the density of hydrogen atoms increases and collisional processes dominate. The total Lyα emission, $j_{tot} \equiv (j_{col} + j_{rec}) \times E_{lya} \times V$ where E_{lya} is the energy of the Lyman α transition and V is the volume of the cell.

3 RESULTS

3.1 Sources of Lyα

For this analysis, we chose to focus on a large halo at z=3 with virial mass $M_* = 3.5\times10^{12} M_\odot$. This halo is not only one of the most massive in the simulation, but its filaments are undergoing a merger, resulting in a large, dense, and Lyα bright filament. An image of the halo in temperature and density is shown in the left panel of Fig. 2 and in total Lyα emission in the right panel. The areas of high temperature and density (orange and light blue, respectively) in the left panel correspond to the highest Lyα emission.

To quantify the dependence of j_{tot} on temperature and gas density, we investigate the phase diagram (temperature vs. gas density) of the gas particles within a box of side length 5 Mpc centered on the halo (as shown in Fig. 2). Our results are shown in Fig. 3. As expected, recombination dominates at high temperatures and low densities while the contribution of collisional excitation is largest at low temperatures and high gas densities; above $\rho \simeq 10^{-2.5}\mathrm{cm}^{-3}$ almost all emission is due to collisions. (The 'tail' feature in the plots in the left column reflects that we impose a polytropic equation of state to prevent artificial fragmentation at high densities where we have insufficient resolution to follow the relevant physics.). From Fig. 3 alone, it is difficult to tell which process is responsible for the majority of emission that is detectable by MUSE. For example, although collisional processes are responsible for the highest levels of Lyα emission, there may be so few particles that undergo this process compared to those undergoing recombination that recombination processes dominate the detectable emission. Fig. 4 addresses this: showing 2d histograms of total,

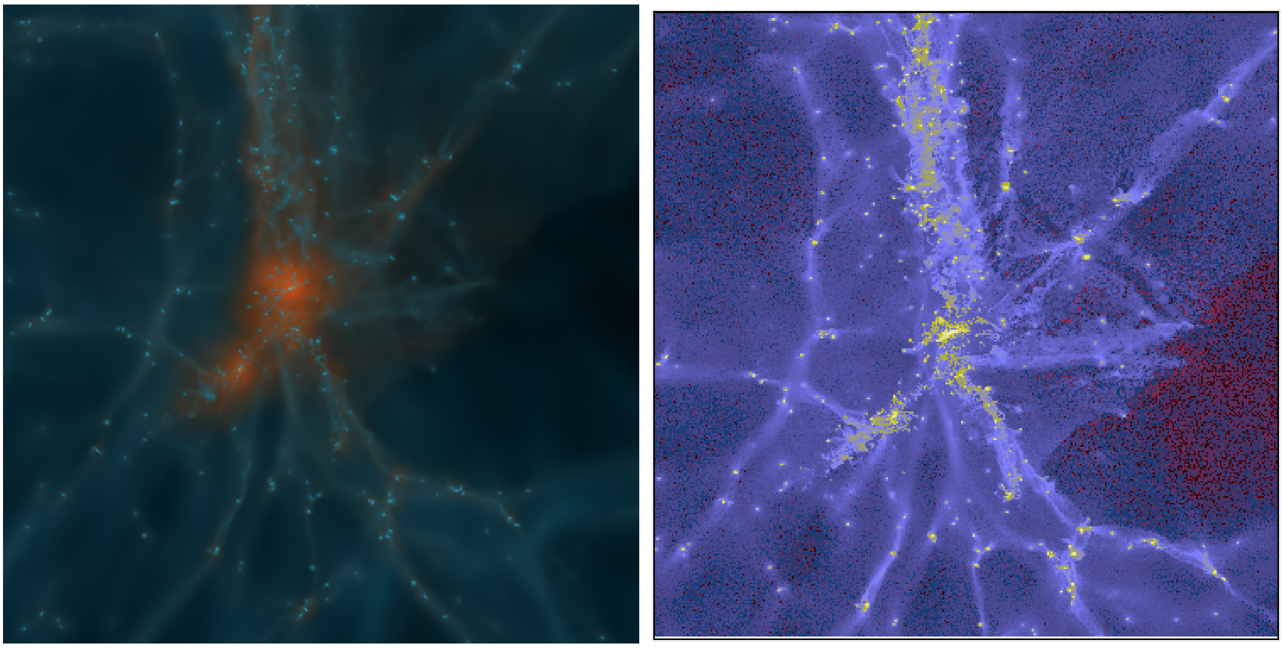

Figure 2. *Left*: Temperature and density map of (5Mpc)^2 region centered on halo created using the low-resolution simulation. Density in blue and temperature in orange. *Right*: Corresponding Lyα emission map. Brightest Lyα emission in yellow. The large filament above the main halo was recently formed by merging two smaller filaments. Star-forming particles are excluded.

collisional, and recombinational emission (from top to bottom) in phase space. The resulting areas of high and low emission are both a reflection of the particle distribution on the phase diagram and levels of emission per particle. The largest amount of detectable emission is due to particles with low temperatures in high-density regions. At these temperatures and densities, collisional processes dominate over recombinational processes. In other words, we predict that most detections of Lyα emission will be due to collisional excitation, in agreement with (Rosdahl and Blaizot 2010). We note that this result is unchanged whether the analysis is performed with low- or high-resolution data.

3.2 Detections with MUSE

We now focus on the detectability of the halo with the MUSE instrument. In Wide Field Mode, MUSE has a spatial sampling of 0.2x0.2 arcsec^2 and a limiting flux in 80 hours of $0.4 * 10^{-19}$ergs^{-1}cm^{-2} (for S/N=5) (Bacon et al. 2017). To test whether a single 80-hour observation of this halo would be sufficient detect any filaments, we create a mock image of the halo in j_{tot}. The halo is located at z=2, but is effectively placed at z=3 by calculating the surface brightness at that distance. Particles associated to any subhalo are removed as we are assuming an optically thin limit and not modeling any self-shielding effects. Including them would strengthen the Lyα emission, thus, the mock image is a lower limit for detection. For the sake of simplicity, the remaining particles are binned in a grid of pixel size consistent with MUSE. To check that the results were not affected by smoothing overdense and underdense areas with the same pixel size, the analysis was also conducted using an SPH method (Benitez-Llambay et al. 2015). As we found no remarkable differences in the results, we use the simpler, binning technique. Fig. 5 shows the resulting mock image with surface dimming taken into account. As expected, the MUSE detection limit is too high to detect any emission.

3.2.1 The Effect of Increased Resolution

A natural step towards boosting the signal is to increase the resolution of the data. To this end we create two images using the low and high resolution simulations, respectively, and smooth them to 30 pixels square. The smoothing is necessary to avoid differences due to small variations in substructure between the two simulations, and is chosen to easily compare with Fig. 7. Pixel values in the high resolution image are boosted by a median factor of ≃1.1 when compared to the low resolution image, with a maximum boost of a factor of 40 and decrement of a factor of 0.05. The top panel of Fig. 6 shows the difference between the high and low-resolution images. Surprisingly, the boosts (and decrements) do not appear to correlate with areas of high (or low) density. For example, the pixels making up the largest, vertical filament directly above the center of the halo in Fig. 7 experience a decrement on average while the pixels in the bottom left filament experience an increment on average. The bottom panel explicitly shows that j_{tot} is no greatly affected by a change in resolution. The pixels that are above the detection limit of MUSE (shaded region) are scattered evenly about the 1:1 relation such that a detectable pixel may experience a boost or decrement with equal probability. While Lyα emission is dependent on the mass of the particles, the effect is canceled by the increase in number of particles per pixel. On average there are a factor of ≃10 more particles in

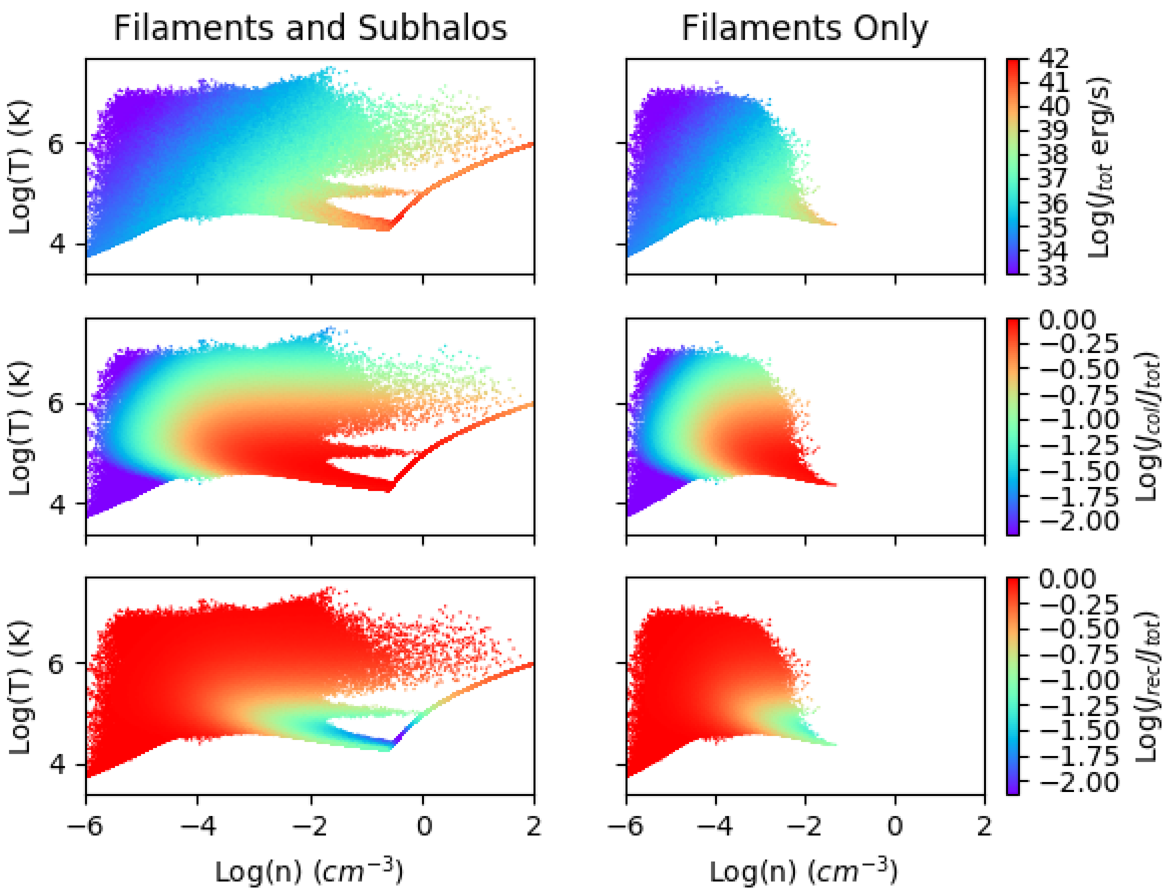

Figure 3. Phase diagrams for gas particles. Left column includes particles bound to halos and subhalos, right column does not. *From top to bottom: Phase space colored by total Lyα emission, fraction of emission due to collisions, and fraction of emission due to recombinations.*

each pixel of the high resolution image, but each particle is a factor of ≃10 less massive. We conclude that changing the resolution of the simulation does not appreciably change the surface brightness levels of the image.

3.3 Degrading Pixel Resolution

Switching to the high resolution simulation does not create a large enough signal boost to reach the MUSE detection limit with a single image. Our next step was to test if by stacking the image on itself, we would be able to reach the limit. We found that on the order of ≃ 10 stacks are required to make a detection. This is untenable for observers not only because each image requires 80 hours of observation, but also because it requires that the images be stacked in such a way that the filaments align, which an observer would not know a priori (see e.g. Steidel et al. (2010)). Our result is in contrast with Gallego et al. (2018), who employ stacking with MUSE data, but are not able to make a detection after 390 'oriented' stacks (subcubes are oriented using positions from nearby Lyα galaxies). However, they suggest that 2/3 of their cubes may not contain filaments. The discrepancy may also be due to the perfect alignment of our stacked images, as well as the unusual brightness of the largest filament.

We thus turn to a different image processing technique: pixel degradation. By decreasing the amount of pixels in an image (effectively combining them), the amount of Lyα photons per pixel is increased, thus increasing the signal. The drawback to this technique is of course the lost information on smaller substructures within the filaments. However, if our main aim is simply to detect a filament, degrading is sufficient for this purpose.

Fig. 7 shows the results of the degrading technique. From Fig. 5, we have reduced the number of pixels from 791^2 to 30^2, corresponding to a change in pixel size from 0.2"^{2} to 5.3"^{2}. This size was chosen to roughly match the width of a typical filament (not the largest filament), and a detection is possible with less degradation. The black contour shows the MUSE detection limit of $10^{-17.8}\mathrm{erg} * \mathrm{s}^{-1} * \mathrm{cm}^{-2}$. With this technique it is possible to detect extended Lyα emission from gas filaments at z=3 with MUSE. Our technique is not new: some examples of degrading pixel resolution to boost signal appear in the literature: Gallego et al. (2018) apply it to MUSE data, increasing the pixel size by a factor of 2. However, to our knowledge, this is the first time degrading has been suggested to such an extent (a factor of 26.5) for use on deep MUSE data.

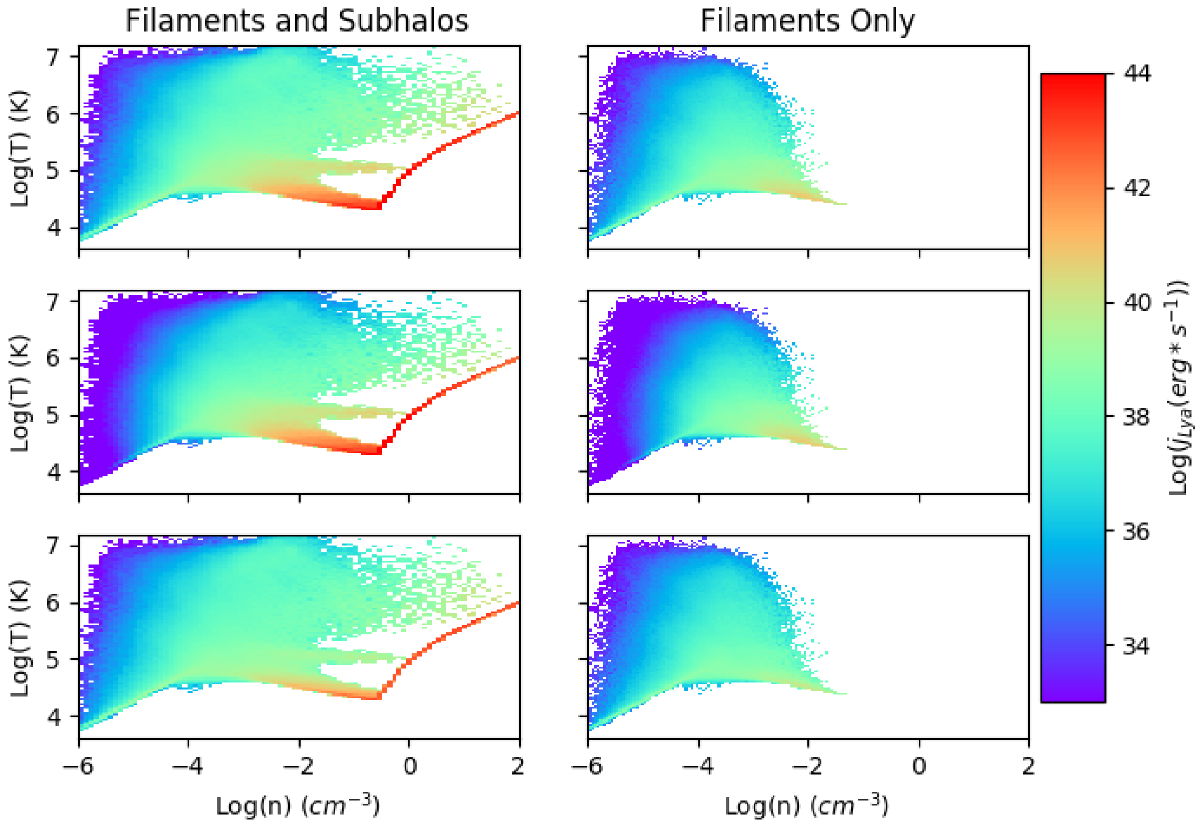

Figure 4. Density of phase space for gas particles. Left column includes particles bound to subhalos, right column does not. *From top to bottom: 2d histograms weighted by total Lyα emission, fraction of emission due to collisions, and fraction of emission due to recombinations.*

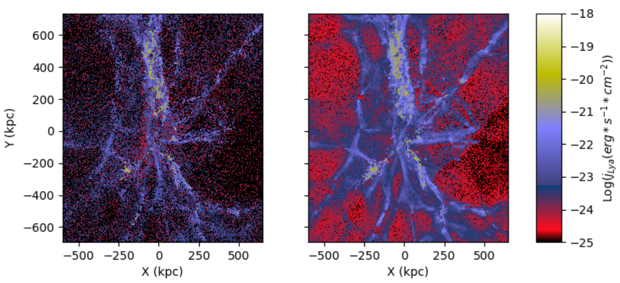

Figure 5. Mock images of total Lyα emission according to MUSE specifications. Low resolution box on left, high resolution box on right. Subhalos are removed. No detection is possible.

4 CONCLUSIONS

We have used two simulations of differing resolutions to investigate the detectability of the filaments feeding a massive ($M_* = 10^{13} M_\odot$) halo at z=3 with the MUSE/VLT instrument. We summarize our findings below:

• Assuming an optically thin limit, we map total Lyα emission (collisional and recombinational) and find it correlates with the temperature and density of the filaments as expected.

• The vast majority of the Lyα emission from gas particles (excluding those in halos and subhalos) in the $(5Mpc)^3$ box centered on the halo is dominated by recombination. This is not surprising due to the fact that most of the gas is ionized. The majority of the *detectable* emission, however, is due to particle collisions in high density areas, in agreement with Rosdahl and Blaizot (2010).

• Overall, a lower particle mass (higher resolution), results in a signal boost by a factor of 1.1. However, the spread is large: some pixels' signals are boosted by a factor of 40 and others are decreased by a factor of 0.05.

• Changing the resolution of the data does not result in a significant signal boost due to the effects of the smaller particle mass being canceled out by the increase in number of particles per pixel.

• Signal boosts or decrements are not correlated with Lyα luminosity.

• Using a single mock image with MUSE specifications we are not able to reach detection limits. Stacking results in eventual detection (after $\simeq$ 10 stacks) but is unfeasible observationally due to the need for the filaments to be exactly oriented in each stack.

• By degrading the pixel resolution of the original mock image by a factor of 26, a detection with MUSE is possible.

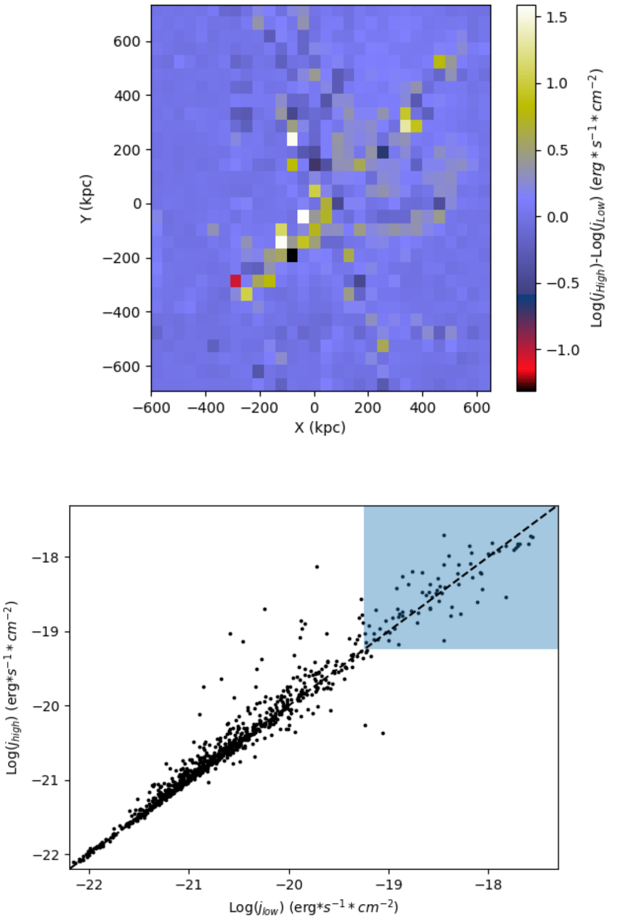

Figure 6. *Top*: Residuals between mock images created with low- and high-resolution data *Bottom*: Dependence of $j_{tot,high}$ on $j_{tot,low}$. (Pixels with j_{tot} = 0 are set to 10^{-27}ergs^{-1}cm−2) The shaded region represents the MUSE detection limit. Dashed line is a 1:1 relation. Scatter in the correlation is larger at higher values of Lyα brightness in the low resolution simulation.

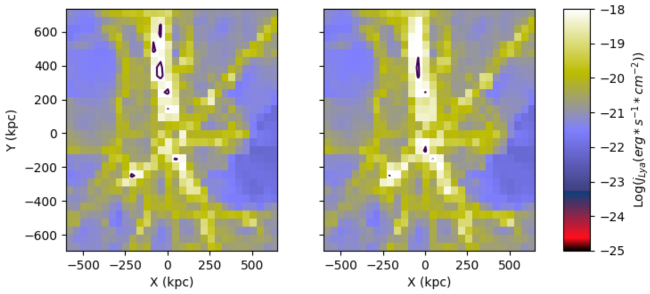

Figure 7. Mock images of total Lyα emission degraded to a pixel size of 5.3”^{2}. Low resolution box on left, high resolution box on right. Subhalos are removed. Contours show MUSE detection limit.

Although we have lost information about small scale structure we are able to detect diffuse gaseous filaments at z=3 to the 5σ level.

4.1 Future Work

Future work will involve extending our analysis to halos of varying masses and environments within the simulation. We intend to characterize of the morphology of the filaments and explore links between their degree of substructure and surface brightnesses. Voronoi mesh methods will be applied as an alternative to our simpler two-dimensional binning technique in order to create mock images and potentially boost signal, given their superior sensitivity to density. Application of our degradation technique on recent and future MUSE data is an exciting avenue for the possible detection of filaments comprising the cosmic web.

ACKNOWLEDGEMENTS

This work was initiated as a project for the Kavli Summer Program in Astrophysics held at the Center for Computational Astrophysics of the Flatiron Institute in 2018. The program was co-funded by the Kavli Foundation and the Simons Foundation. We thank them for their generous support.

REFERENCES

Bacon R. et al., 2017, A&A, 608, A1
Battaia A. et al., 2018, MNRAS, 473, 3907A
Benitez-Llambay A., py-sphviewer: Py-SPHViewer v1.0.0, http://dx.doi.org/10.5281/zenodo.21703
Dekel A. et al., 2009, Nature, 475, 451
Dolag K. et al., 2009, MNRAS, 399, 497
Dijkstra M., 2017, arXiv: 1704.03416
Fardal M. A. et al., 2001, ApJ, 562, 605
Faucher-Giguere C. et al., 2010, ApJ, 725, 633
Gallego S. et al., 2018, MNRAS, 475, 3854
Haider M. et al., 2016, MNRAS, 457,3024
Hinshaw G. et al., 2013, ApJ, 208, 19
Klypin, A. A. and Shandarin, S. F. , 1983, MNRAS, 204,891
Osterbrock D.E and Ferland G. J., 2006, Astrophysics of Gas Nebulae and Active Galactic Nuclei, University Science Books
Peebles P. J. E., Groth E. J., 1975, ApJ, 196,1
Rosdahl J. and Blaizot J., 2012, MNRAS, 423, 344
Springel V. et al., 2001, MNRAS, 328, 726
Springel V. and Hernquist, L., 2003, MNRAS, 339, 289
Springel V., 2010, MNRAS, 401, 791
Steidel C C. et al., 2010, ApJ, 717, 289S
Swinbank A. M. et al., 2015, MNRAS, 449, 1298
Vogelsberger M. et al., 2014, MNRAS, 444, 1518
Zheng C. et al., 2018, ApJ, 861, 1

This paper has been typeset from a TEX/LATEX file prepared by the author.